Original Article

Institution of MECHANICAL ENGINEERS
Journal of ENGINEERING IN MEDICINE

Proc IMechE Part H:
J Engineering in Medicine
2023, Vol. 237(7) 890–904

DOI: 10.1177/09544119231181246
journals.sagepub.com/home/pih
Sage

A novel rat-tail model for studying human finger vibration health effects

Ren G Dong, Christopher Warren, Xueyan S Xu, John Z Wu, Daniel E Welcome, Stacey Waugh and Kristine Krajnak

Abstract

It has been hypothesized that the biodynamic responses of the human finger tissues to vibration are among the major stimuli that cause vibration health effects. Furthermore, the finger contact pressure can alter these effects. It is difficult to test these hypotheses using human subjects or existing animal models. The objective of this study was to develop a new rat-tail vibration model to investigate the combined effects of vibration and contact pressure and to identify their relationships with the biodynamic responses. Physically, the new exposure system was developed by adding a loading device to an existing rat-tail model. An analytical model of the rat-tail exposure system was proposed and used to formulate the methods for quantifying the biodynamic responses. A series of tests with six tails dissected from rat cadavers were conducted to test and evaluate the new model. The experimental and modeling results demonstrate that the new model behaves as predicted. Unlike the previous model, the vibration strain and stress of the rat tail does not depend primarily on the vibration response of the tail itself but on that of the loading device. This makes it possible to quantify and control the biodynamic responses conveniently and reliably by measuring the loading device response. This study also identified the basic characteristics of the tail biodynamic responses in the exposure system, which can be used to help design the experiments for studying vibration biological effects.

Keywords

Hand-arm vibration, hand-transmitted vibration, rat-tail vibration model, vibration-induced white finger, hand-arm vibration syndrome

Date received: 9 December 2022; accepted: 24 May 2023

Introduction

The operation of powered hand tools and the machining of handheld workpieces can generate significant vibrations. Prolonged and intensive exposure to such vibrations may cause a series of vascular, neurological, and musculoskeletal disorders in the hand-arm system, which are collectively termed hand-arm vibration syndrome (HAVS).[1,2] Vibration-induced white finger (VWF), or cold-induced finger blanching, is the hallmark symptom of HAVS. Previous studies have formed a great body of knowledge in this research area and helped develop several standards and guidelines for helping assess the risk of vibration exposure and control health effects.[1–4] However, as stated in a standard,[4] "the vibration exposures required to cause these disorders are not known precisely, neither with respect to vibration magnitude and frequency spectrum nor with respect to daily and cumulative exposure duration." The hand forces may significantly affect the vibration transmission and health effects,[5–8] but they have not been considered in the current standard for assessing the risk of vibration exposure, because quantitative relationships between hand forces and health effects have not been established.

According to structure failure theories,[9,10] biomechanics,[11] and conceptual models of the human vibration exposure and health effects,[1,12] the biodynamic responses such as the vibration stresses, strains, and power absorption density (VPAD) of the tissues in the hand-arm system should be associated with the psychophysical, physiological, and pathological responses of

Physical Effects Research Branch, Health Effects Laboratory Division, National Institute for Occupational Safety and Health (NIOSH), Morgantown, WV, USA

Corresponding author:
Ren G Dong, Physical Effects Research Branch, Health Effects Laboratory Division, National Institute for Occupational Safety and Health (NIOSH), 1095 Willowdale Road, MS L-2027, Morgantown, WV 26505, USA.
Email: rkd6@cdc.gov

the system to vibration. The specific roles of the biodynamic responses in the development can be examined by testing the following hypothesis: (i) the biodynamic responses of finger tissues are among the major factors that cause psychophysical, physiological, and pathological effects of the finger vibration exposure; and (ii) the finger grip force or contact pressure can directly or indirectly modulate these effects because the stress and strain resulting from the finger contact pressure can change the finger vibration transmissibility, tissue biodynamic properties, blood circulation, and nerve function. Although similar concepts or hypotheses have been proposed over the years[13,14] and a few analytical studies have been performed,[15–17] our literature search did not identify studies that experimentally examined the quantitative relationships among the biodynamic responses, fingers-applied force, and biological effects. The exact relationship between these exposure factors has been far from clearly identified and understood. Systematic investigations of this fundamental scientific gap may lead to some breakthroughs in this research area and effectively address the above-described issues.

For ethical and technical reasons, it is difficult to study the biological effects of vibration exposure using human subjects, especially when looking at factors that contribute to the development of pathology. Instead, biological or animal models have been used to examine the relationship between vibration exposure factors and their physiological and pathological effects and these studies contributed to our understanding of the mechanisms leading to dysfunction and injury.[12,18–22] The rat-tail model has been frequently used in these studies, probably because it is the most practical model and the tail has some biodynamic and biological similarities to the human finger.[23] Published studies have found that the biological effects of vibration on rat tails were frequency-dependent, characterized by an increase in markers of injury and dysfunction in the fundamental resonant frequency range.[19,20] This may be primarily because the vibration stresses and strains in the resonant frequency range are higher than those in the non-resonant frequency range. However, the quantitative relationship between vibration stresses/strains and biological effects has not been examined, because it is difficult to quantify the tissue stresses and strains of the tail in these rat-tail models.

The previous rat-tail models have partially simulated the finger contact pressure, as the tail is kept in contact with the platform at least at the strapped locations. It has been reported that increasing the number of straps from 4 to 7 in the rat-tail model increased the biological effects under a 5 g sinusoidal excitation.[24] This suggests that it is important to include the static force in such a vibration study. However, a systematic investigation of its influences on biological effects has not been conducted. It is difficult to use the strap method to apply and control the contact pressure consistently and accurately on the tail.

Overall, it is difficult to use previous animal models, including the previous rat-tail models, to examine the quantitative relationships between biodynamic responses and biological effects. As the first step to systematically address the fundamental scientific gap in this research area, the objective of this study is to develop a new rat-tail model for further studying finger vibration health effects and their relationships with the finger biodynamic responses. While the preliminary results of the study have been reported in a conference abstract,[25] the updated development and experimental results are presented in this paper.

Design, construction, and analysis of the new rat-tail model

The new rat tail model includes two parts: (i) a new rat-tail vibration exposure system; and (ii) a set of methods for quantifying the rat-tail pressure and vibration exposures.

Design and construction of the new rat-tail vibration exposure system

The new rat-tail exposure system was developed by adding a loading device to the existing NIOSH rat-tail vibration exposure system,[23] as illustrated in Figure 1. The loading plate is placed on the middle portion (typically from the C12-18 vertebrate) of the rat tail which is secured on the vibration platform using elastic straps. The loading plate can apply both static and dynamic/vibration forces on this portion of the tail so that much more vibration-induced stress and strain can be generated in the tissues in this tail portion than in the other portions of the tail under the same excitation.

As illustrated in Figure 2, the loading device is composed of a loading plate, four uniform loading springs, and four poles for installing the device on the vibration platform. Each of the poles is locked on the platform with a nut. The other nuts on each pole are used to adjust the compressed length of the spring to control the static force applied on the tail through the loading plate. Two sets of springs were used to achieve different ranges of the applied force: Set 1 from 0.25 to 2.5 N; Set 2 from 1 to 8 N. The loading plate has a groove with a cone-like shape, which can conform better to the reduced diameter along the tail and secure the tail to the vibration platform. The groove on the plate was covered with a thin layer of rubber (about 0.5 mm) to adapt to the tail and reduce the potential of undesired traumatic injury. The vibration force on the tail depends primarily on the mass and acceleration of the loading plate. The plate mass can be changed by adjusting the plate height.

The loading plate was fabricated using a 3D printer with polylactic acid filament. The printed guide holes were rough, which could increase the friction force of

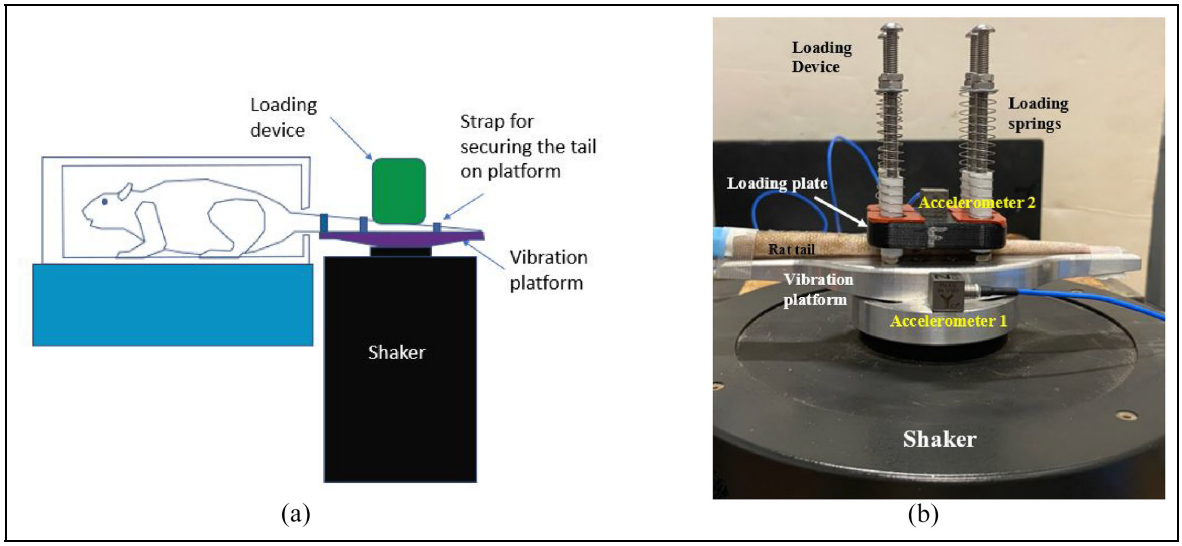

Figure 1. A proposed new rat tail vibration exposure system for studying finger vibration health effects: (a) general system design and (b) a pictorial view of the exposure system.

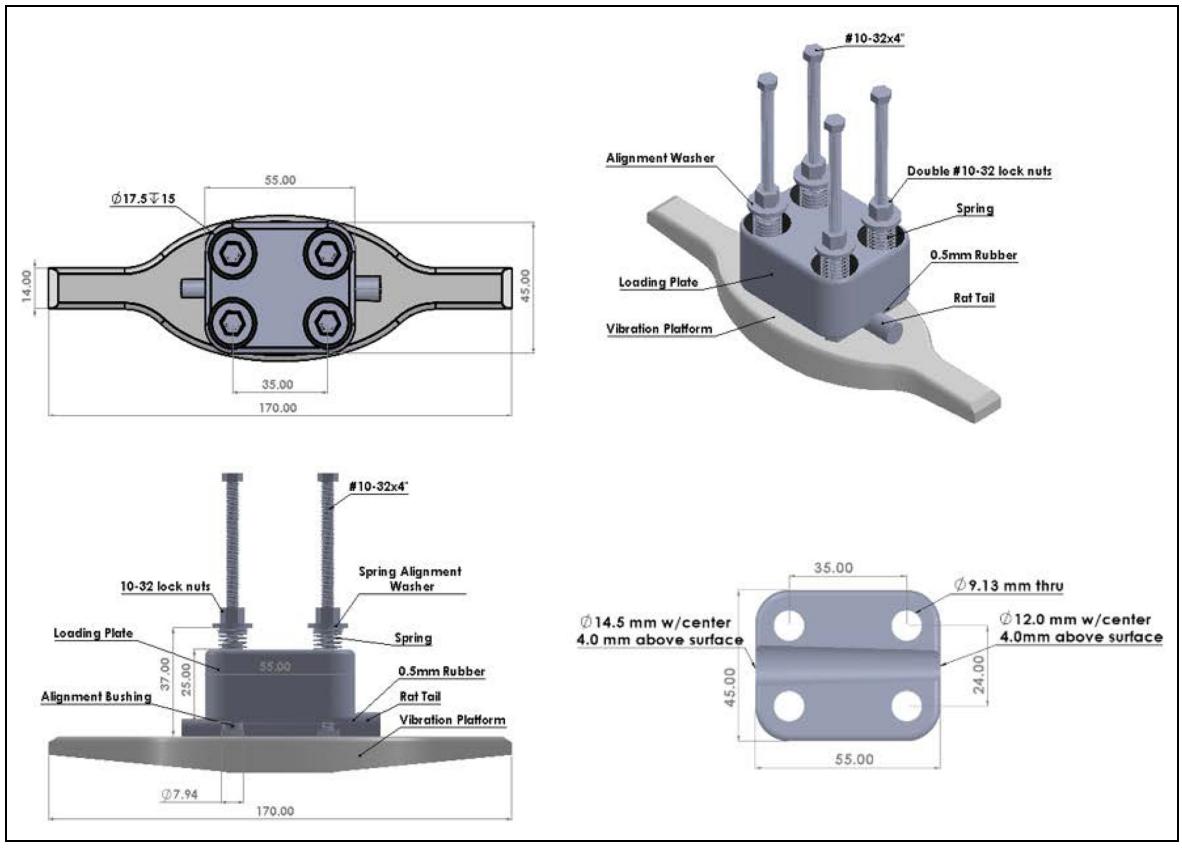

Figure 2. Technical design of the loading device.

the loading device. This issue was resolved by making the diameter of each hole slightly smaller than its designed dimension for 3D printing and expanding it using a drill and further smoothing it using fine sanding paper. Some mineral oil was applied to the holes to further minimize the friction force. The vibration platform can be fixed on a shaker or a vibrating tool through an adapter. In the current study, the vibration platform with the loading device was installed on a single-axis shaker (B&K, 4808) for all the vibration tests performed in this study. As shown in Figure 1(b), Accelerometer 1 (PCB, 356A12) is fixed on the vibration platform using cyanoacrylate glue, and Accelerometer 2 (PCB, 356B11) is on the loading plate.

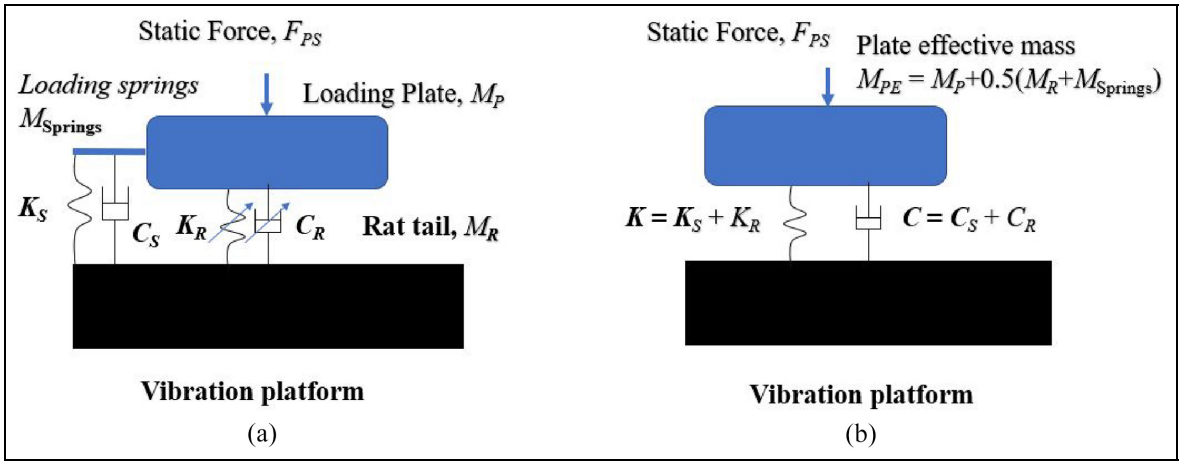

Figure 3. Analytical models of the new rat-tail vibration exposure system: (a) nonlinear model and (b) linear model.

Methods for quantifying the rat tail pressure and vibration exposures

The rat-tail exposure system was simulated using a lumped-parameter model with a single degree of freedom (1-D), which is illustrated in Figure 3(a). The four identical loading springs were represented by K_S ($= 4k_{\text{Spring}}$). Half of their mass ($0.5M_{\text{Springs}}$) was lumped into the loading plate. The damping value of the loading device was represented by C_S, which could primarily result from the friction between the loading plate and its guides on the poles. The tail was represented by a spring-damper element in the model, as the mass of the loaded tail portion ($M_R < 3$ g) is much less than that of the loading plate and it can be ignored or partially lumped into the loading plate. The stiffness (K_R) and damping value (C_R) of the tail generally vary with the force (F_{PS}) applied on the tail. If the force remains unchanged, these tail properties can be locally linearized. Hence, the model shown in Figure 3(a) can be simplified into a linear 1-D model shown in Figure 3(b), which was mostly used in this study.

Quantifications of static and vibration pressures/stresses and strains of the tails. So far, it has been unknown which biomechanical measure is more closely associated with vibration health effects. As static and dynamic stresses and strains have been commonly used in the designs and analyses of engineering structures,[9,10] they should be among the potential measures for studying the human vibration exposures.

The pressure or stress is defined as the force per unity area on or in a structure.[9] The average static contact pressure ($\sigma_{\text{Ave-S}}$) was estimated using the static force (F_{PS}) and the tail contact area that was estimated from the average tail contact width (b_t) and length (L_t):

$$\sigma_{\text{Ave-S}} \approx \frac{F_{PS}}{b_t \cdot L_t} \tag{1}$$

Similarly, the average magnitude of the contact vibration stress ($\sigma_{\text{Ave-D}}$) was estimated using the vibration force ($\boldsymbol{F}_{PR}$) acting on the tail and the tail contact area:

$$\sigma_{\text{Ave-D}} \approx \frac{|\boldsymbol{F}_{PR}|}{b_t \cdot L_t} \tag{2}$$

For the linear model shown in Figure 3(b), the vibration force on the tail was estimated from:

$$\boldsymbol{F}_{PR} = M_{PE}\boldsymbol{A}_P - [K_S(\boldsymbol{D}_P - \boldsymbol{D}_V) + C_S(\boldsymbol{V}_P - \boldsymbol{V}_V)], \tag{3}$$

where $\boldsymbol{D}_P$ and $\boldsymbol{D}_V$ are the complex displacements of the plate and platform, respectively; $\boldsymbol{V}_P$ and $\boldsymbol{V}_V$ are their corresponding velocities; and $\boldsymbol{A}_P$ and $\boldsymbol{A}_V$ are their corresponding accelerations. Substituting equation (3) into equation (2) and considering the relationships among the displacement, velocity, and acceleration ($\boldsymbol{D} = \boldsymbol{A}/[j\omega]^2$, $\boldsymbol{V} = \boldsymbol{A}/[j\omega]$, $j = \sqrt{-1}$), the average dynamic contact stress can be estimated from

$$\sigma_{\text{Ave-D}} \approx \left| M_{PE}A_V \cdot \boldsymbol{T}_P - \left[\frac{K_S}{(2\pi f)^2} + \frac{jC_S}{2\pi f}\right] A_V(1 - \boldsymbol{T}_P)\right| / (b_t \cdot L_t), \tag{4}$$

where $\boldsymbol{T}_P$ ($= \boldsymbol{A}_P/\boldsymbol{A}_V$) is the transfer function of the loading plate. Because the phase angle of the reference or platform acceleration can be assumed zero, $\boldsymbol{A}_V = A_V$.

The strain is a measure of the material deformation per unit length or angle in a structure.[9] In this study, the cross-section of a tail in its loaded portion was assumed an approximate circle with an average diameter of d_t. When the maximum deformation of the tail (δ or Δd_t) in its loaded portion is measured or estimated, the maximum static strain ($\varepsilon_{\text{Max-S}}$) can be estimated from

$$\varepsilon_{\text{Max-S}} \approx \frac{\Delta d_t}{d_t} \tag{5}$$

Similarly, the average vibration strain ($\varepsilon_{\text{Ave-D}}$) in the vibration direction can be estimated from

$$\varepsilon_{\text{Ave-D}} \approx \frac{|(\boldsymbol{D}_P - \boldsymbol{D}_V)|}{h_t} = \frac{\left|\frac{\boldsymbol{A}_V - \boldsymbol{A}_P}{\omega^2}\right|}{h_t} = \frac{|(1 - \boldsymbol{T}_P)A_V|}{(2\pi f)^2 h_t} \quad (6)$$

where h_t is the height of the deformed tail in the vibration direction.

Quantifications of the rat-tail vibration exposure. As the tail biodynamic properties under a static force can be locally linearized, the tail structure can be considered approximately a linear system in the vibration exposure. Hence, the vibration stress (σ) in the loaded tail portion can be assumed approximately proportional to the vibration contact pressure expressed in equation (2)[9]:

$$\sigma \approx \Omega \cdot \sigma_{\text{Ave-D}}, \quad (7)$$

where Ω is the stress proportional factor.

The development of musculoskeletal disorders resulting from mechanical hazards exposures can be conceptually consider a long-term fatigue process.[12,26] Hence, like the method widely used in the fatigue analysis of engineering structures,[10] the proposed stress method assumes the vibration health effects are associated with the stress magnitude and the number of the stress cycle over the exposure duration (T). Hence, its related vibration exposure dose (Γ_σ) at each frequency (f) can be written as follows:

$$\Gamma_\sigma = \sigma \cdot f^\lambda \cdot \text{T} = \Omega \cdot \ I_\sigma \cdot \text{T}, \quad (8)$$

where λ is termed as stress frequency weighting ($\leqslant 1.0$), and I_σ is termed as vibration stress dose index expressed as follows:

$$I_\sigma = \sigma_{\text{Ave-D}} \cdot f^\lambda \quad (9)$$

Like the stress method, the proposed strain method also assumes that the vibration strain (ε) inside the tail for a given static force is approximately proportional to the average vibration strain expressed in equation (6):

$$\varepsilon \approx Q \cdot \varepsilon_{\text{Ave-D}}, \quad (10)$$

where Q is the strain proportional factor. Like the stress method, the strain method also assumes the vibration health effects are associated with the strain magnitude and the number of the strain cycle. Hence, its related vibration exposure dose (Γ_ε) can be written as follows:

$$\Gamma_\varepsilon = \varepsilon \cdot f^\gamma \cdot \text{T} \approx Q \cdot \ I_\varepsilon \cdot T \quad (11)$$

where γ is termed as strain frequency weighting ($\leqslant 1.0$), and I_ε is termed as vibration strain dose index expressed as follows:

$$I_\varepsilon = \varepsilon_{\text{Ave-D}} \cdot f^\gamma \quad (12)$$

It has been proposed to use the vibration power absorption (VPA) as an alternative measure to quantify the hand-arm vibration exposure.[13] While it has been demonstrated that the total VPA is like the standard frequency-weighted acceleration method and may not be suitable for studying the finger vibration effects,[27] the vibration power absorption per unit volume of tissue or VPA density (VPAD) has been proposed to study the effects.[28] Like the vibration stress and strain, the VPAD method assumes the distributed VPAD in the tail is approximately proportional to the average VPAD of the entire loaded tail portion for a given static force. With the model shown in Figure 3(b), the total vibration power absorption of the loaded tail portion can be estimated from the dynamic force ($\boldsymbol{F}_{RC} = C_R \cdot \boldsymbol{\Delta V}$) and the velocity difference ($\boldsymbol{\Delta V} = \boldsymbol{V}_P - \boldsymbol{V}_V$). Then, the average VPAD = $\boldsymbol{F}_{RC} \cdot \boldsymbol{\Delta V}/v = C_R \cdot (\boldsymbol{V}_P - \boldsymbol{V}_V)^2/v$, where v is the volume of the loaded tail ($v \approx 0.25\pi d_t^2 \cdot L_t$). The general VPAD at any point in the tail can be expressed as follows:

$$\text{VPAD} \approx P \cdot \frac{\boldsymbol{C_R} \cdot |\boldsymbol{V}_P - \boldsymbol{V}_V|^2}{\nu}, \quad (13)$$

where P is a proportional factor of the VPAD. The VPAD method assumes that the biological effects are associated with the vibration energy absorbed by the tail tissues for a given period (T). Hence, the vibration exposure dose for the energy method (Γ_{VPAD}) can be written as follows:

$$\begin{aligned} \Gamma_{VPAD} &= \text{VPAD} \cdot \text{T} \approx P \cdot \frac{\boldsymbol{C_R} \cdot |\boldsymbol{V}_P - \boldsymbol{V}_V|^2}{\nu} \cdot \\ &\text{T} = P \cdot \ I_{VPAD} \cdot \text{T}, \end{aligned} \quad (14)$$

where I_{VPAD} is termed as VPAD dose index, which can be expressed as follows:

$$I_{VPAD} = \frac{C_R \cdot \left[\frac{|(\boldsymbol{T}_P - 1)A_V|}{2\pi f}\right]^2}{v} \quad (15)$$

Testing and evaluation of the new rat tail exposure system

The major criteria for assessing the success of the new exposure system are as follows: (i) the vibration response of the loading device or the transfer function of the loading plate can be reliably measured and closely simulated using the 1-D model shown in Figure 3(b); and (ii) the parameters of the exposure system can be reliably measured or estimated using practical and convenient methods. While the mass parameters (M_P, M_{Springs}, M_R) and spring stiffness (K_S) of the analytical

model were separately measured, a series of tests and modeling analyses were conducted to determine the damping value of the loading device (C_S). Another series of tests and modeling analyses were conducted to measure the transfer function of the loading plate in a rat tail vibration exposure and to determine the tail stiffness (K_R) and damping value (C_R). The contact width of each tail was measured and used to estimate the static deformation, stress, and strain of the tail.

Damping tests and modeling analyses of the loading device

In the damping test, the rat tail shown in Figure 1(b) was replaced with a set of eight springs with a length of about 6 mm. They were placed in parallel between the loading plate and the vibration platform. Their compressed length was like the compressed height of the rat tail in the exposure system. Two series of damping tests were conducted. The first one used the loading device equipped with the first set of springs and the initial loading plate. The applied static force in this series of tests was 2.23 N. The testing variables included three sinusoidal excitations (2.73, 4.88, and 6.84 m/s^2) at each of the one-third octave bands from 20 to 500 Hz. The second series of tests used the second set of springs and the updated loading plate. The testing variables included three forces (1.41, 3.54, 6.09 N) and three levels of sinusoidal excitations (3.48, 5.21, 8.0 m/s^2). Each excitation was controlled using a closed-loop control program (MB Dynamics, WIN2k5-5GB). Two trials were performed for each test treatment. The transfer function of the loading plate at each frequency was measured using a data acquisition system (B&K 3050/3053) and the data averaged for 6 s were recorded.

Figure 4 shows examples of the transfer functions measured in the damping tests, together with their corresponding modeling results. The analytical model shown in Figure 3(b) was used in the modeling analysis. The tail stiffness and damping value were replaced with the short spring stiffness ($K_{SS} = K_R$) and damping value ($C_{SS} = C_R$). Because the damping value of the springs should be very small, it was ignored or $C_{SS} \approx 0$; hence, $C = C_S + C_{SS} \approx C_S$. Then, the C_S and K_{SS} values were estimated by fitting the modeling transfer function to the experimental data using a model calibration method.[29] The modeling transfer function was calculated using the formula for a 1-D model described in a handbook,[30] and the modeling was performed in MS Excel. As shown in Figure 4, the modeling results generally agree very well with the experimental data. The estimated damping values are listed in Table 1, together with their corresponding damping ratios ($\zeta = C_{SS}/[2M_{PE} \cdot 2\pi f_n]$, where $f_n = 0.5[K/M_{PE}]^{1/2}/\pi$). The damping values varied randomly in a large range (from 0.95 to 5.07 N s/m) with a mean of 3.55 for the first series of tests and 2.50 N s/m for the second series of tests. This suggests that the device's damping value has some uncertainties. However, the damping ratios were generally small, especially for the updated loading device, which is also reflected from the features of the spectra presented in Figure 4.

Rat tail tests and modeling analyses

The basic testing setup and instrumentation used in the rat tail tests were the same as those used in the damping tests, except that six real tails were used in the tests. These tails were dissected from rat cadavers from the studies that examined the effects of inhaling particulate matter. These rats had served as air controls in these studies and the procedures used to expose them were performed as described in a protocol approved by the institutions Animal Care and Use Committee. The diameters and mass values of the tails in their loaded portions are listed in Table 2. The updated design of loading plate shown in Figure 2 was used in the tests. Two variables were considered in the tests, which include two applied forces (2.21 and 4.59 N), three levels of sinusoidal excitation (3.48, 5.21, 8.00 m/s^2) at each of the frequencies from 20 to 1000 Hz in the one-third octave bands. While the first set of loading springs was used for the test at the 2.21 N static force, the second set of springs was used for the test at the 4.59 N static force. The vibration transfer function of the loading plate for 5 s at each frequency was measured. Two trials were performed for each treatment. The sequence of the test treatments was randomized among the six tails.

The measured transfer functions, together with their corresponding modeling responses, are presented in Figure 5. Similar to determine the damping value of the loading device, the tail stiffness and damping value were estimated using a model calibration method with the model shown in Figure 3(b).[29] The parameters required in the modeling and the estimated K_R and C_R values are listed in Table 3 for each tail and their corresponding natural frequencies and damping ratios are listed in Table 3. The results indicate that increasing the static force significantly increased the tail stiffness and damping value, as well as the system natural frequency, but reduced the system damping ratio ($p < 0.001$). Increasing the excitation marginally reduced the tail stiffness ($\leqslant 16\%$; $p = 0.006$) and the system natural frequency ($\leqslant 8.4\%$; $p = 0.002$), but it did not significantly affect the damping value of the rat rail and the system damping ratio ($p \geqslant 0.38$). There was no significant interaction between the static force and excitation for any of the dependent variables.

Measurement of tail contact width and estimations of tail static strain and stress

The loaded portion of each tail was dissected and used to measure its mass and contact width with the flat vibration platform. The pictorial views of the width measurement setup and contact marker are shown in

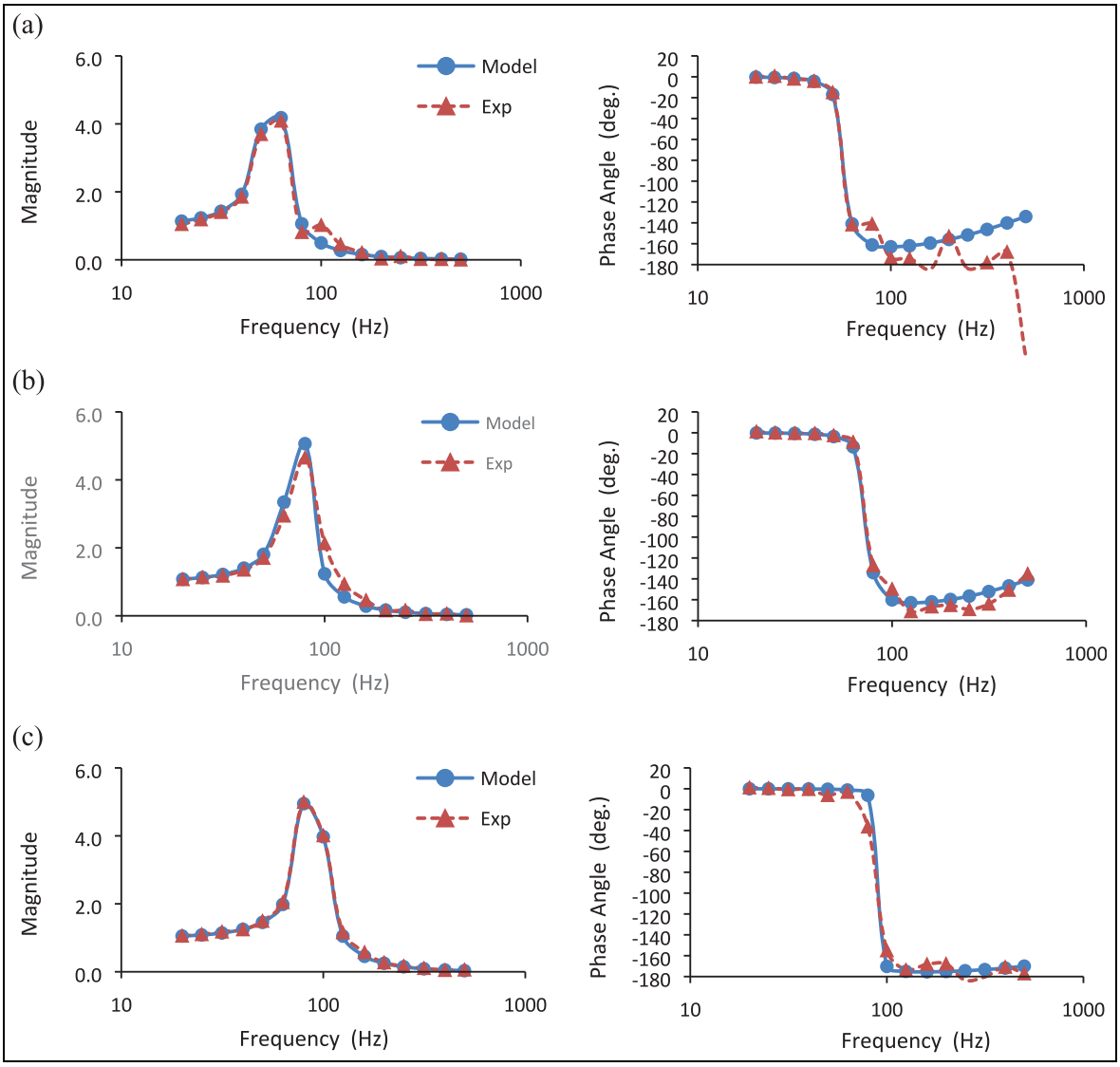

Figure 4. The vibration transfer functions of the loading plate measured in the damping test with an excitation (A_V = 5.21 m/s^2) under three static forces (1.41, 3.54, and 6.09 N): (a) F_{PS} = 1.41 N, (b) F_{PS} = 3.54 N, and (c) F_{PS} = 6.09 N.

Figure 6(a) and (b). The tail was laid in the groove of the loading plate. A piece of flat plastic glass (11.2 g) was positioned on the tail. A light level was glued on the glass to maintain a stable contact with the tail. Two calibrated weights (each with 200 g) were used as the loads; hence, three static forces (0.11, 2.07, and 4.03 N) were applied in the measurement. The measured contact widths (b_t) are listed in Table 4. A trendline ($b_t = 4.0723F_{PS}^{0.2033}$) fits these data very well ($R^2 = 0.9999$). The trendline was used to estimate the contact widths for the two static forces (2.21 and 4.59 N) used in the rat tail vibration tests, which are also listed in Table 4.

The maximum tail deformation (δ) should be at the flat contact interface. It was estimated from the tail contact width using a crude model illustrated in Figure 6(c). The estimation was based on the following assumptions: (a) the deformations of the platform and loading plate can be ignored because they are much

Table 1. The damping values and ratios of the loading device for different testing treatments identified from the modeling of the transfer functions measured in the damping tests.

First series of tests	Applied force (N)	Excitation (m/s^2)		
		2.73	4.88	6.84
Damping value, C_S (N s/m)	2.23	2.88	3.47	4.30
Damping ratio, ζ	2.23	0.09	0.10	0.13
Second series of tests	**Applied force (N)**	**Excitation (m/s^2)**		
		3.48	5.21	8.0
Damping value, C_S (N s/m)	1.41	1.80	2.33	4.71
	3.54	5.01	3.02	1.77
	6.09	1.02	0.95	1.79
Damping ratio, ζ	1.41	0.04	0.06	0.12
	3.54	0.09	0.06	0.03
	6.09	0.02	0.02	0.03

Table 2. The diameters and mass values of the rat tails underneath the loading plate.

Animal ID	Proximal diameter (mm)	Distal diameter (mm)	Mean diameter (d_t) (mm)	Tail mass of loaded portion (L_t = 53 mm), M_R (g)
1	8.5	6.5	7.50	2.27
2	8.5	6.0	7.50	2.34
3	8.0	6.5	7.25	2.34
4	7.5	6.5	7.00	2.26
5	8.0	6.5	7.25	2.25
6	8.0	5.5	6.75	2.47
Mean	8.1	6.3	7.21	2.32

stiffer than the rat tail; (b) the cross-section of the loaded tail portion has a circular profile with a diameter before (d_t) and after the deformation (D_t); (c) because the tail tissues are incompressible, the deformed area of the tail is equal to the original area of the tail or $0.5\pi(\frac{D_t}{2})^2 - \theta(\frac{D_t}{2})^2 + 0.5b_t h_{t-P} = 0.5\pi(\frac{d_t}{2})^2$, in which $\sin(\theta) = \frac{b_t}{D_t}$ and $h_{t-P} = D_t cos(\theta)$. After D_t and h_{t-P} are resolved for a given b_t with these equations, the maximum deformation can be estimated from $\delta = \frac{d_t}{2} - h_{t-P}$. The estimated contact parameters are listed in Table 4, together with the estimated average static contact pressure/stress ($\sigma_{\text{Aver-static}} = F_{SP}/[b_t L_t]$) and maximum static strain of the tail ($\varepsilon_{\text{Max}-\text{static}} = \delta/h_{t-P}$).

Characteristics of the rat tail biodynamic responses and exposure dose indexes

Figure 7 illustrates the rat tail vibration contact stress and strain calculated using equations (4) and (6), with the transfer functions shown in Figure 5 and the related parameters listed in Tables 3 and 4. The shape of each stress spectrum was like that of the vibration transmissibility (the magnitude of transfer function). As expected, the dynamic contact stress generally increased with the increase in the excitation. It reached the maximum value at the resonant frequency of the loading system. Increasing the static load shifted the resonance to a higher frequency; The basic trends of the strain spectra were like those of the stress spectra. However, increasing the static force substantially reduced the resonant strain.

The exposure dose indexes for the three methods were calculated using equations (9), (12), and (15), respectively. As dictated by equations (5) and (9), the vibration stress or strain dose index is simply the multiplication of the stress or strain by a weighted frequency. While the frequency weightings could not be determined in this study, they were assumed unity or $\lambda = \gamma = 1.0$ in the index calculations for exploring the basic characteristics of the dose index spectra. The calculated index spectra are plotted in Figure 8(a) and (b). Because increasing the frequency increases the number of vibration cycles, the relative weighting or importance of the stress or strain dose index at a higher frequency was more than that evaluated based on the vibration stress or strain. The VPAD index is more sensitive to the excitation than the stress and strain indexes.

To further identify the major differences among the three methods, the index spectrum for each testing treatment was normalized with respect to its resonant peak. The results are plotted in Figure 9. The peak frequencies of the three methods were similar. The stress and strain methods were similar to each other below the resonant frequency, but the stress method took a higher weighting beyond the resonant frequency. The VPAD method had a much higher weighting in the resonant frequency range that the other two methods.

Discussions

General assessment of the new rat-tail vibration model

The results of this study demonstrate that the new rat-tail model can provide a reasonable simulation of the combined static and dynamic environments of the finger vibration exposure in a tool operation. The natural frequencies listed in Table 3 represent the resonant frequencies of the vibration force acting on the rat tails under different testing treatments. They are in the range of the finger natural frequencies.[8,31–33] If necessary, the fundamental natural frequency of the fingers under a given contact force can be closely simulated in the rat-tail model by adjusting the mass of the loading plate. The static force effects on the system responses shown in Figure 5 are similar to those of the grip force on the finger vibration response.[8,32] The tail vibration stress was generally several times less than that of its static stress, as shown in Figure 7 and Table 4; this is comparable with the relationship between the finger dynamic force and the grip force.[34] Also shown in these figure and table, the tail dynamic strain was less than 0.0027, which was much less than that of its static strain (0.21–0.28); this feature is also likely to be similar to that of the finger tissue strains. The results of this study also demonstrated that the biodynamic responses of the tail can be quantified and controlled conveniently and reliably by measuring and controlling the vibration

Table 3. The stiffness and damping value of the rat tail and the natural frequency and damping ratio of the loading device estimated from the modeling of the plate transfer functions measured in the rat tail tests under three excitations and two loading forces.

Parameter	A_V (m/s^2)	Test 1 (with the first set of springs): F_{PS} = 2.21 N, K_S = 53 N/m, C_S = 2.5 Ns/m, $M_{Springs}$ = 1.6 g, M_R = 2.32 g, M_P = 51.6 g						
		Tail 1	Tail 2	Tail 3	Tail 4	Tail 5	Tail 6	Mean
Tail stiffness,	3.48	93,440	110,006	107,876	139,434	112,735	100,218	110,618
K_R (N/m)	5.21	102,355	107,128	90,854	110,479	102,110	109,685	103,769
	8.00	101,878	75,383	101,913	108,599	71,917	98,561	93,042
Tail damping value,	3.48	19.87	21.98	23.14	26.92	18.84	18.30	21.51
C_R (N s/m)	5.21	20.56	19.92	22.21	22.37	18.04	19.28	20.40
	8.00	21.61	18.87	22.30	21.25	14.96	19.68	19.78
Natural frequency,	3.48	210	228	225	256	231	217	228
f_n (Hz)	5.21	220	225	207	228	219	227	221
	8.00	219	188	219	226	184	216	209
Damping ratio, ζ	3.48	0.16	0.16	0.17	0.17	0.14	0.14	0.16
	5.21	0.16	0.15	0.18	0.16	0.14	0.14	0.15
	8.00	0.16	0.17	0.17	0.16	0.14	0.15	0.16
Parameter	A_V (m/s^2)	Test 2 (with the second set of springs): F_{PS} = 4.59 N, K_S = 236 N/m, C_S = 2.5 Ns/m, $M_{Springs}$ = 6.1 g, M_R = 2.32 g, M_P = 51.6 g						
		Tail 1	Tail 2	Tail 3	Tail 4	Tail 5	Tail 6	Mean
Tail stiffness,	3.48	274,210	212,883	244,062	278,307	262,037	315,137	264,439
K_R (N/m)	5.21	208,612	234,797	263,147	277,086	271,562	279,121	255,721
	8.00	236,563	240,777	263,748	216,520	200,208	273,915	238,622
Tail damping value,	3.48	29.18	25.83	28.35	31.16	27.09	38.25	29.98
C_R (N s/m)	5.21	27.04	28.30	30.61	30.34	27.54	33.98	29.63
	8.00	29.41	28.57	31.75	29.37	26.08	32.44	29.60
Natural frequency,	3.48	352	310	332	355	344	378	345
f_n (Hz)	5.21	307	326	345	354	351	355	340
	8.00	327	330	346	313	301	352	328
Damping ratio, ζ	3.48	0.13	0.13	0.13	0.13	0.12	0.15	0.13
	5.21	0.14	0.13	0.14	0.13	0.12	0.15	0.13
	8.00	0.14	0.13	0.14	0.14	0.13	0.14	0.14

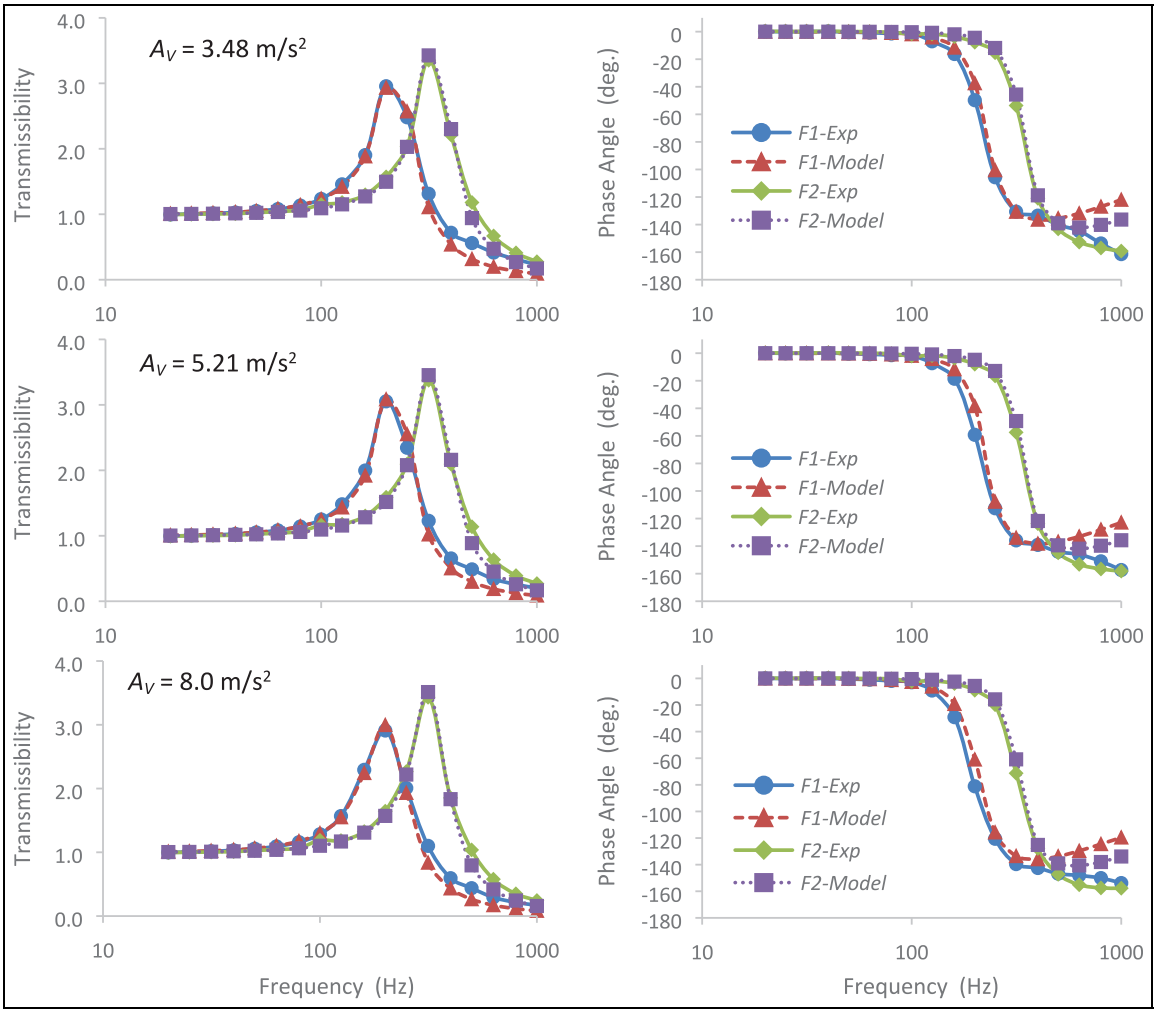

Figure 5. The comparisons of the mean transfer functions of the six rat tails simulated (Model) and measured (Exp) under the two static forces ($F1 = 2.21$ N; and $F2 = 4.59$ N) and three excitations ($A_V = 3.48$, 5.21, and 8.0 m/s^2).

transfer function of loading plate. Hence, the new rat-tail model is acceptable for investigating the quantitative relationships between biodynamic responses and biological effects under combined pressure and vibration exposures.

A major concern was that the contact pressure applied to the tail with the loading plate could block blood circulation. This concern did not become an issue in the initial application of the new model to investigate the biological effects of the applied pressure.[35] Similar to the static forces used in the current study, 2 N static force was applied in the animal study. This force increased the blood flow and did not cause traumatic injury to the tails.[35] This suggests the loading device and its designed force range are acceptable for biological experiments.

The characteristics of the biodynamic responses shown in Figures 7 and 8 can be used to help design the experiments for studying vibration biological effects. The dose index formulas (equations (9) and (12)) for stress and strain methods suggest that the vibration frequency may affect the biological effects in two different ways: (a) the frequency determines the vibration stress and strain magnitudes; they reach their maximum values at the fundamental resonant frequency, as shown in Figure 7; and (b) the frequency determines the number of cyclic force or deformation actions per second, which affect the exposure dose indexes, as shown in Figure 8. These two different roles may result in different frequency dependencies of the biological effects. The first role can be identified by examining the relationship between the vibration stress/strain and the biological effects when the different platform accelerations at the same frequency are used in a biological experiment. The second role can be identified by examining the biodynamic-biological relationship when the vibration stress or strain is controlled at the same level at different frequencies. This testing condition can be achieved by controlling the acceleration on the loading plate at the same level at different frequencies. Such experimental studies can be used to determine the stress and strain frequency weightings (λ and γ) in equations (9) and (12).

Table 4. The tail contact width (b_t) and contact parameters estimated form mean width value: contact area (= $b_t \cdot L_t$), average contact pressure/stress ($\sigma_{Ave-D} = F_{PS}/[b_t \cdot L_t]$), maximum deformation ($\delta$), deformed half tail height (h_{t-P}), and maximum strain ($\varepsilon_{Max-S} = \delta/h_{t-P}$).

F_{PS} (N)	Tail ID and measured contact width, b_t (mm)							$b_t \cdot L_t$ (mm^2)	σ_{Ave-D} (kPa)	δ (mm)	h_{t-P} (mm)	ε_{Max-S}
	1	2	3	4	5	6	Mean					
0.11			3.44	1.86	3.17	1.92	2.60	138	0.80	0.22	3.38	0.06
2.07	5.21	4.79	5.91	4.11	3.93	4.49	4.74	251	8.25	0.73	2.87	0.20
4.03	5.99	5.46	6.28	5.07	4.49	5.09	5.39	286	14.10	0.95	2.65	0.26
2.21*							4.78**	254	8.72	0.75	2.86	0.21
4.59*							5.55**	294	15.60	1.01	2.59	0.28

*Static force used in the tail tests. **Estimated from the trendline: $b_t = 4.0723(F_{PS})^{0.2033}$

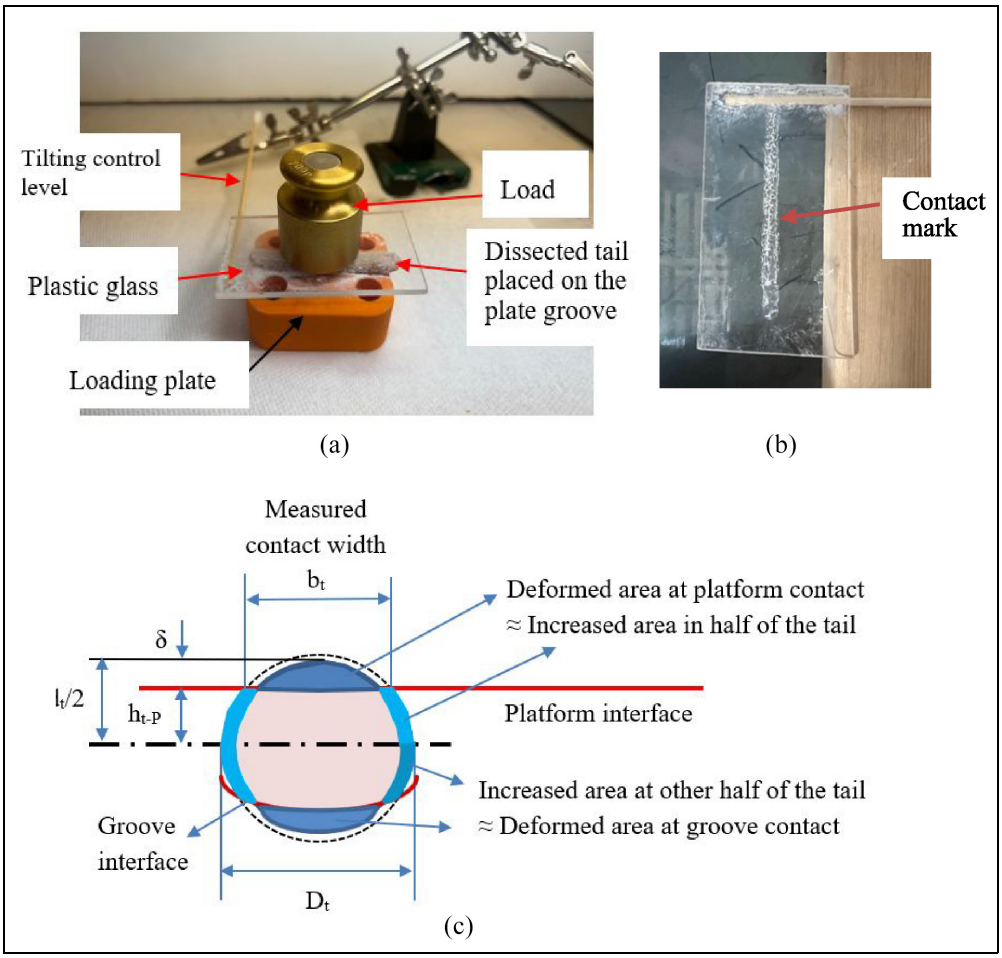

Figure 6. The method for measuring tail contact width and the method for crudely estimating the contact deformation from the measured contact width: (a) measurement of tail contact width, (b) a sample of contact marker, and (c) estimation of tail contact deformation.

Limitations and potential improvements of the rat-tail exposure system

The current version of the rat-tail vibration exposure system has some limitations and can be improved. The loading device is applicable primarily for the vibration exposure in the vertical vibration direction. The device at a low static force (< 0.5 N) may not work very well at more than 160 Hz, as found from the initial experiment with the original loading device.[25] This may be primarily because the tail stiffness and damping values are small at the low force level and the high frequency vibration may not be effectively transmitted to the plate. As shown in Table 3, the damping value of the loading device may vary randomly in a certain range. The rat-tail damping value at the low force level fall into this range, which may reduce the reliability of the estimated model parameters and the biodynamic responses. Hence, it is recommended to use 1 N or higher static force in the applications of the new rat-tail

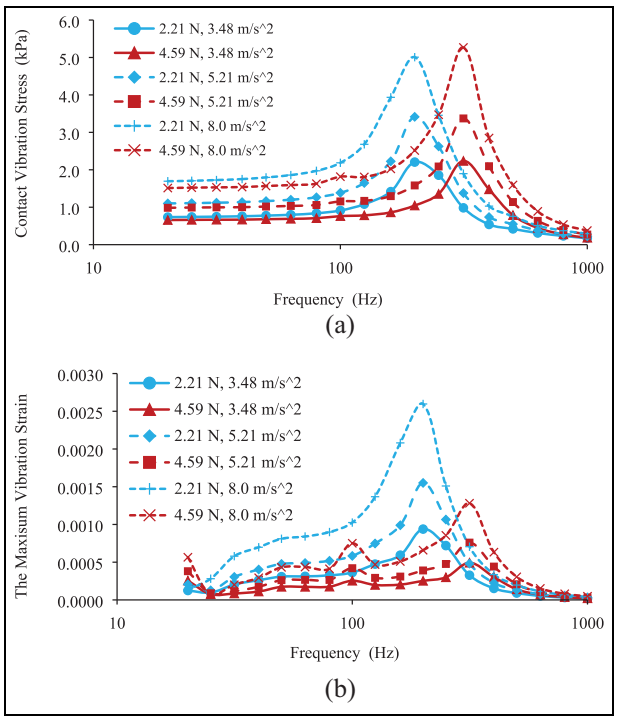

Figure 7. Comparisons of the rat tail contact vibration stresses and strains under two static forces ($F1 = 2.21$ N; and $F2 = 4.59$ N) and three excitations ($A_V = 3.48$, 5.21, and 8.0 m/s^2): (a) rat tail contact vibration stress and (b) rat tail vibration strain.

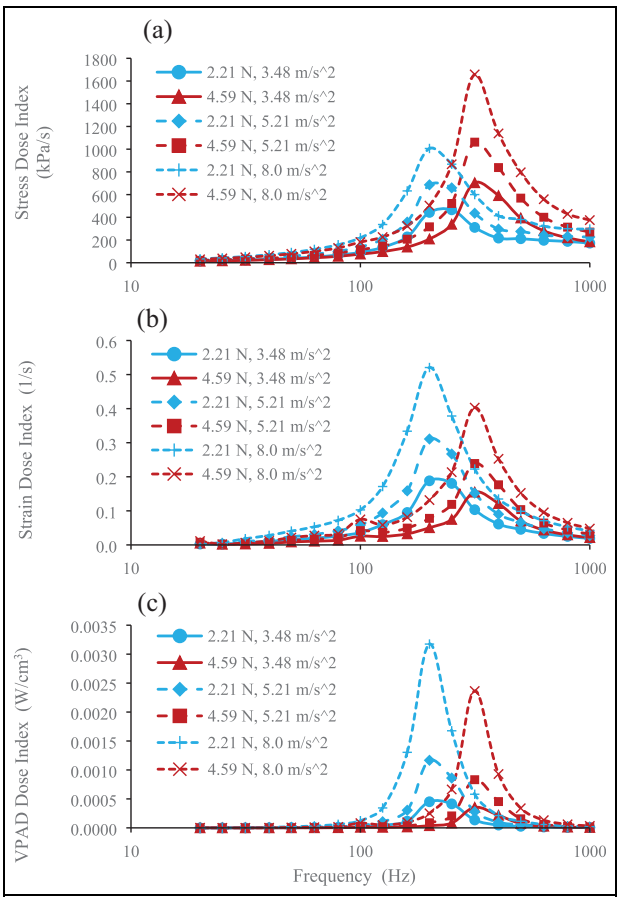

Figure 8. Comparison of the rat tail vibration exposure dose indexes of three methods under two quasi-static forces (2.21 and 4.59 N) and three excitations (3.48, 5.21, and 8.0 m/s^2): (a) stress method, (b) strain method, and (c) VPAD method.

model. At such force levels, the damping value of the rat tails is likely to be much larger than that of the loading device, as shown in Tables 1 and 3. The random damping factor is unlikely to substantially affect the estimated responses of the rat tails, as demonstrated in the preliminary study.[25] Maintaining the guides with mineral oil can keep the damping value of the loading device at a low level.

The loading springs used in this study have a resonant frequency at about 100 Hz, which resulted in a small but undesired resonant peak in the biodynamic responses in some cases, as shown in Figure 7. If this frequency is required in a biological investigation, an alternative set of springs that have no resonance at this frequency should be considered.

Limitations and potential improvements of the methods for quantifying tail vibration exposure

The proportional factor (Ω, Q, or P) for quantifying the biodynamic responses and exposure doses could not be determined in this study, as it is difficult to experimentally determine them. A comprehensive finite element (FE) model of the rat tail is required to estimate the distributed biodynamic responses and these factors. The determinations of these proportional factors may not be essential if only the overall biodynamic responses of the tail are of concern, especially in the initial investigation on the quantitative relationship between the biodynamic responses and biological effects. In such cases, the dose index can be used to approximately represent the tail vibration exposure for a given exposure duration; it can be directly used to examine the relationship between the biodynamic responses and the biological effects. In other words, if any of the biodynamic measures is associated with the biological effects, the association should be at least partially reflected in their correlation.

The method shown in Figure 6(a) for measuring the tail contact area may not be accurate. The method shown in Figure 6(c) for estimating the tail deformation may be less accurate. While these inaccuracies are unlikely to change the basic characteristics of the tail biodynamic responses, they can be improved in further studies. The force-deformation relationship may be measured using the method similar to that used in the soft tissue experiment.[36] Such information is also required for the development of the FE model.

Like any engineering structure,[9,10] the static and dynamic responses of the rat tail tissues during the pressure and vibration exposures are generally in all

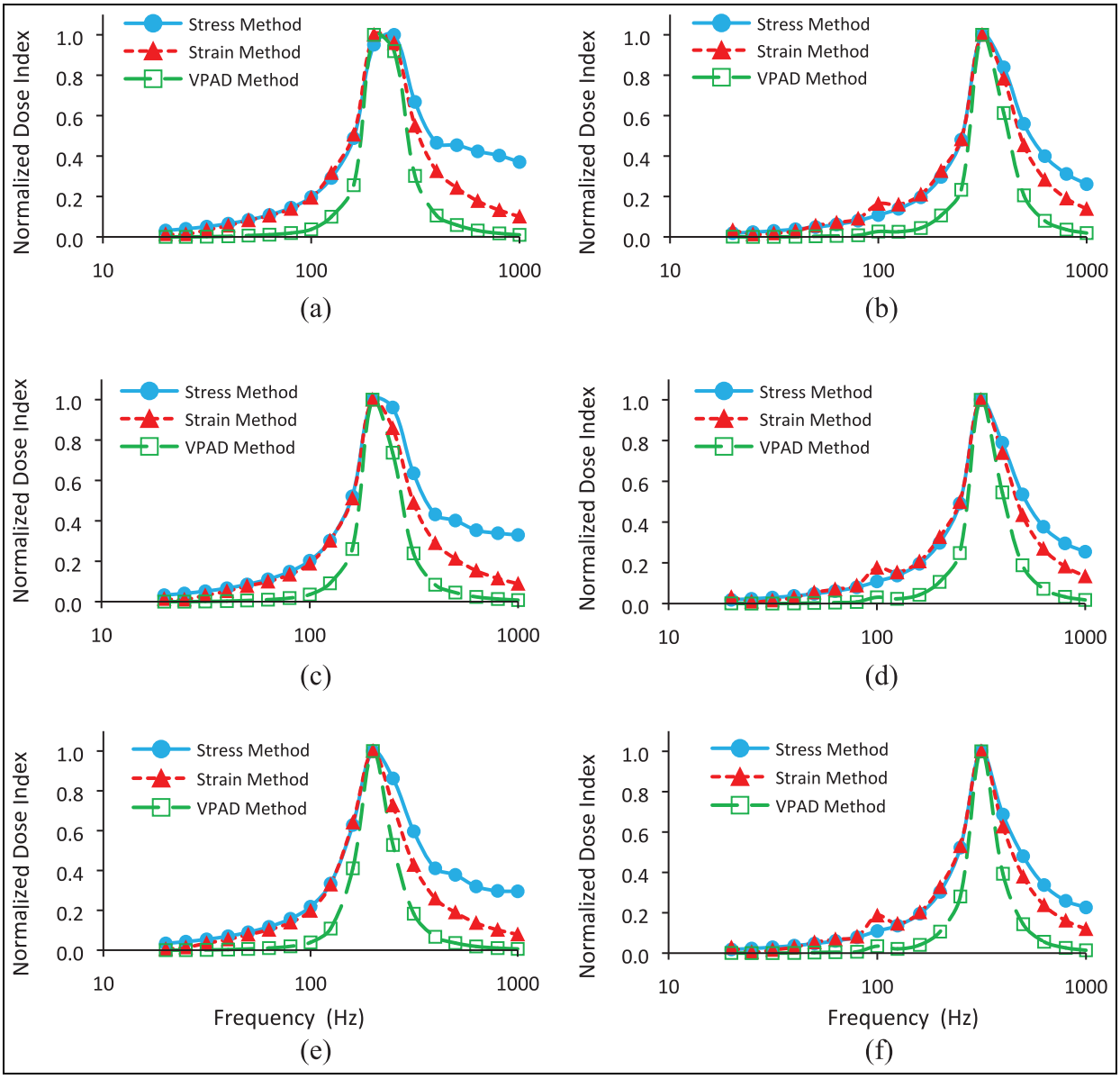

Figure 9. Comparison of the exposure dose indexes normalized with respect to the resonant peak for each of the three methods (stress, strain, and VPAD methods): (a) $F_{PS} = 2.21$ N, $A_v = 3.48$ m/s^2, (b) $F_{PS} = 4.59$ N, $A_v = 3.48$ m/s^2, (c) $F_{PS} = 2.21$ N, $A_v = 5.21$ m/s^2, (d) $F_{PS} = 4.59$ N, $A_v = 5.21$ m/s^2, (e) $F_{PS} = 2.21$ N, $A_v = 8.0$ m/s^2, and (f) $F_{PS} = 4.59$ N, $A_v = 8.0$ m/s^2.

directions with both normal and shear components. This study used only the normal component in the excitation direction as a base for quantifying the responses. This is an efficient approach, but the quantified responses may not be fully representative of the biomechanical environment of the tail tissues. The inaccuracy or possible errors, however, should not affect the general validity of this approach, because the major static and dynamic responses are in the excitation direction and the responses in the other directions are likely to be correlated with the normal component in the excitation direction. Hence, the estimated responses and their related exposure dose indexes can be used to explore and establish preliminary relationships between the responses and biological effects. The relationships can be verified and/or improved when more accurate responses are quantified.

Conclusions

This study developed a novel rat-tail model for investigating how vibration and applied force may affect the risk of developing vibration-induced health effects in human fingers. A loading device was developed to apply static and vibration forces on the middle portion of a rat tail constrained on a vibration platform. A set of formulas were developed to quantify the tail vibration exposure based on the vibration stress, strain, and power absorption density of the tail tissues. The results of this study demonstrate that the new rat-tail vibration exposure system can provide a reasonable simulation of the human finger vibration exposure. This study also demonstrated that the biodynamic responses of the rat tail can be controlled and quantified by measuring the

vibration response on the loading device. The identified characteristics of the biodynamic responses provide useful information for the design of the rat-tail experiments for studying the finger vibration health effects.

Declaration of conflicting interests

The author(s) declared no potential conflicts of interest with respect to the research, authorship, and/or publication of this article.

Funding

The author(s) disclosed receipt of the following financial support for the research, authorship, and/or publication of this article: This study was funded by US NIOSH NORA program (9390KK1).

Disclaimers

The findings and conclusions in this manuscript are those of the authors and do not necessarily represent the official position of the National Institute for Occupational Safety and Health, Centers for Disease Control and Prevention.

ORCID iD

Ren G Dong https://orcid.org/0000-0003-0574-5522

References

1. Griffin MJ. *Handbook of human vibration*. London: Academic Press, 1990, p.988.
2. Pelmear PL and Wasserman DE. *Hand-arm vibration: a comprehensive guide for occupational health professionals*. 2nd ed. Beverly Farms, MA: OEM Press, 1998.
3. ANSI. *ANSI S2.70: guide for the measurement and evaluation of human exposure to vibration transmitted to the hand (Revision of ANSI S3.34-1986)*. New York, NY: American National Standards Institute (ANSI), 2006.
4. ISO 5349-1. *Mechanical vibration—measurement and evaluation of human exposure to hand-transmitted vibration—part 1: general requirements*. Report no. ISO 5349-1:2001, 2001. Geneva, Switzerland: International Organization for Standardization.
5. Adewusi SA, Rakheja S, Marcotte P, et al. Vibration transmissibility characteristics of the human hand-arm system under different postures, hand forces and excitation levels. *J Sound Vib* 2010; 329: 2953–2971.
6. Kihlberg S. Biodynamic response of the hand-arm system to vibration from an impact hammer and a grinder. *Int J Ind Ergon* 1995; 16: 1–8.
7. Pyykkö I, Färkkilä M, Toivanen J, et al. Transmission of vibration in the hand-arm system with special reference to changes in compression force and acceleration. *Scand J Work Environ Health* 1976; 2: 87–95.
8. Dong JH, Dong RG, Rakheja S, et al. A method for analyzing absorbed power distribution in the hand and arm substructures when operating vibrating tools. *J Sound Vib* 2008; 311: 1286–1304.
9. Ye J. *Structural and stress analysis: theories, tutorials and examples*. 2nd ed. New York, NY: CRC Press, 2015.
10. Schijve J. *Fatigue of structures and materials*. 2nd ed. Dordrecht: Springer, 2008.
11. Taber LA. Biomechanics of growth, remodeling and morphogenesis. *Appl Mech Rev* 1995; 48: 487–545.
12. Dong RG, Wu JZ, Xu XS, et al. A review of hand-arm vibration studies conducted by US NIOSH since 2000. *Vibration* 2021; 4: 482–528.
13. Lidström IM. Vibration injury in rock drillers, chiselers, and grinders. Some views on the relationship between the quantity of energy absorbed and the risk of occurrence of vibration injury. In: *Proceedings of the international conference on hand-arm vibration*, pp.77–83. NIOSH-publication 1977, Cincinnati, OH, USA.
14. Dong RG, Schopper AW, McDowell TW, et al. Vibration energy absorption (VEA) in human fingers-hand-arm system. *Med Eng Phys* 2004; 26: 483–492.
15. Wu JZ, Krajnak K, Welcome DE, et al. Analysis of the dynamic strains in a fingertip exposed to vibration: correlation to the mechanical stimuli on mechanoreceptors. *J Biomech* 2006; 39: 2445–2456.
16. Wu JZ, Dong RG, Rakheja S, et al. A structural fingertip model for simulating the biomechanics of tactile sensation. *Med Eng Phys* 2004; 26: 165–175.
17. Wu JZ, Krajnak K, Welcome D, et al. Analysis of the biodynamic interaction between the fingertip and probe in the vibrotactile tests: the influences of the probe/fingertip contact orientation and static indentation. *J Biomech* 2009; 42: 116–124.
18. Krajnak K, Riley DA, Wu J, et al. Frequency-dependent effects of vibration on physiological systems: experiments with animals and other human surrogates. *Ind Health* 2012; 50: 343–353.
19. Krajnak K, Miller GR, Waugh S, et al. Characterization of frequency-dependent responses of the sensorineural system to repetitive vibration. *J Occup Environ Med* 2012; 54: 1010–1016.
20. Krajnak K, Waugh S, Miller GR, et al. Vascular responses to vibration are frequency dependent. *Indian J Occup Environ Med* 2010; 52: 584–594.
21. Loffredo MA, Yan JG, Kao D, et al. Persistent reduction of conduction velocity and myelinated axon damage in vibrated rat tail nerves. *Muscle Nerve* 2009; 39: 770–775.
22. Curry BD, Govindaraju SR, Bain JL, et al. Evidence for frequency-dependent arterial damage in vibrated rat tails. *Anat Rec A Discon Mol Cell Evol Biol* 2005; 284: 511–521.
23. Welcome DE, Krajnak K, Kashon ML, et al. An investigation on the biodynamic foundation of a rat tail vibration model. *Proc IMechE, Part H: J Engineering in Medicine* 2008; 222: 1127–1141.
24. Krajnak K, Miller GR and Waugh S. Contact area affects frequency-dependent responses to vibration in the peripheral vascular and sensorineural systems. *J Toxicol Environ Health, A* 2018; 81: 6–19.
25. Dong RG, Warren C, Wu JZ, et al. Development of a novel rat tail model for studying human finger vibration health effects. In: *The 15th international conference on hand-arm vibration*, Nancy, France, 6–9 June 2023.
26. Gallagher SS and Schall MC Jr. Musculoskeletal disorders as a fatigue failure process: evidence, implications and research needs. *Ergonomics* 2017; 60: 255–269.

27. Dong RG, Welcome DE, McDowell TW, et al. Frequency weighting derived from power absorption of fingers-hand-arm system under z_h-axis vibration. *J Biomech* 2006; 39: 2311–2324.
28. Dong RG, Wu JZ, Welcome DE, et al. Estimation of vibration power absorption density in human fingers. *J Biomech Eng* 2005; 127: 849–856.
29. Dong RG, Welcome DE, McDowell TW, et al. Theoretical foundation, methods, and criteria for calibrating human vibration models using frequency response functions. *J Sound Vib* 2015; 356: 195–216.
30. Harris CM. *Shock and vibration handbook*. New York, NY: McGraw-Hill, 1996.
31. Griffin MJ, Macfarlane CR and Norman CD. The transmission of vibration to the hand and the influence of gloves. In: AJ Brammer and W Taylor (eds) *Vibration effects on the hand and arm in industry*. New York, NY: John Wiley & Sons, 1982, pp.103–116.
32. Welcome DE, Dong RG, Xu XS, et al. The effects of vibration-reducing gloves on finger vibration. *Int J Ind Ergon* 2014; 44: 45–59.
33. Xu XS, Welcome DE, Warren C, et al. An evaluation of experimental methods for measuring the vibration transmissibility of vibration-reducing gloves at or on the fingers. In: *The 14th international conference on hand-arm-vibration*, Bonn, Germany, 2019.
34. Dong RG, Welcome DE and Wu JZ. Estimation of biodynamic forces distributed on the fingers and the palm exposed to vibration. *Ind Health* 2005; 43: 485–494.
35. Krajnak KW, Warren C, Xu XS, et al. Effects of applied pressure on sensorineural and peripheral vascular function in an animal model of hand-arm vibration syndrome. In: *The 15th international conference on hand-arm vibration*, Nancy, France, 6–9 June 2023.
36. Wu J, Dong RG and Smutz WP. Characterization of nonlinear and time-dependent behavior of skin under compression. In: J Vossoughi (ed.) *Biomedical engineering recent developments*. Washington, DC: Medical and Engineering Publishers, Inc., 2002, pp.187–188.